CD4 T lymphocyte counting on a Microfluidic Chip

Utkan Demirci[1,3,6], Meredith Dixon[2], Palaniappan Sethu[3], Lee Zamir[2], Daniel Irimia[3], Xuanhong Cheng[3], Berthold K. Horn[4], William Rodriguez[2,5], Mehmet Toner[3,6]

[1]BAMM Labs, Bio-Acoustic-MEMS in Medicine, Brigham and Women's Hospital, Harvard Medical School, Cambridge, Massachusetts, 02139

[2]Partners AIDS Research Center, Massachusetts General Hospital, Boston, Massachusetts, 02115

[3]Massachusetts General Hospital, Harvard Medical School, and Shriners Hospital for Children, Boston, Massachusetts, 02114

[4] Massachusetts Institute of Technology, Cambridge, Massachusetts, 02139

[5]Division of AIDS, Harvard Medical School and Department of Medicine, Brigham and Women's Hospital, Boston, Massachusetts, 02115

[6]Harvard-Massachusetts Institute of Technology Health Sciences and Technology, MA 02138

mtoner@sbi.org , wrodriguez@partners.org, udemirci@rics.bwh.harvard.edu

Abstract

Effective antiretroviral therapy (ART) for HIV is now widely available, and more than 1.3 million people worldwide are currently receiving ART. The CD4 cell count, representing the number of CD4+ T lymphocytes per milliliter of blood, is used to evaluate HIV infection, define treatment eligibility and monitor patients. In clinical laboratories, this information is obtained by laser flow cytometry. There is a critical need for simple, reliable, low-cost HIV diagnostic tools that could be utilized in low-income countries, where resources are scarce. We describe a method to incorporate a porous filter into a microfluidic chip in order to separate and count $CD4^+$ T lymphocytes from whole blood. This device utilizes only 1 μL of blood and captures CD4 cells in less than 60 seconds. Fluorescence imaging and digital image analysis provide a CD4 count in less than 3 minutes. An initial prototype device operation is presented. Fabricated devices are characterized with beads and with whole blood from healthy volunteers and from HIV-infected subjects.

Introduction

More than 30 million HIV-infected people live in the developing world. In 2002, the U.S. National Intelligence Council (NIC) predicted that the number of HIV-infected individuals in the developing world would rise to 80 million by 2010[1]. Effective antiretroviral therapy (ART) for HIV has been available in developed countries for more than a decade. Worldwide, 1.3 million people are currently receiving treatment[1]s. To increase access to HIV care and to improve treatment outcome, there is an urgent need for low-cost diagnostic tools[2-7] that could be implemented in developing countries[4, 8, 9].

The absolute number of $CD4^+$ T lymphocytes in blood is vital when evaluating HIV-infected patients. The CD4 count has important prognostic and therapeutic implications. The CD4 count is used to determine when to initiate treatment as well as to monitor the response to treatment. For instance, a healthy adult has a range of CD4 counts averaging around 1000 cells per microliter of whole blood[2, 5]. Clinically, a CD4 count below 200 cells per microliter establishes the diagnosis of AIDS. Since HIV-infected people are at risk for severe opportunistic infections, in most settings ART treatment is initiated at this critical value[10]. Guidelines recommend that patients be monitored routinely for CD4 counts every 3 months in the developed world, and every 6 months in low-income countries.

The World Health Organization has stated that there is an urgent need for a handheld, reliable, low-cost CD4 counting device for use in resource-scarce regions of the world. In high-income settings, CD4 counts rely on flow cytometry, which utilizes lasers to excite fluorescent cell markers[4, 8]. Flow cytometry provides the gold standard in CD4 analysis[11, 12] that could cost less than two US dollars. Here, we present a technology that has the potential in the future to create assays for lower cost. A point-of-care CD4 count device could allow obtaining this vital information in resource limited settings.

There have been recent efforts to develop affordable CD4 counting methods by adapting flow cytometry such as the Partec and Guava systems[12]. These devices are more affordable than standard flow cytometers. There are other emerging techniques for CD4 counts. Beyond district hospitals and for point-of-care use in developing countries, systems that do not involve several sample preparation steps, and that are not labor intensive, are attractive[7, 13-17]. Previously, Rodriguez *et al.* reported on a new approach to CD4 counting, and described a large-scale laboratory prototype that combined a stainless steel flow cell and plastic tubing with digital fluorescence imaging[4]. This prototype required sample preparation and incubation off-chip and multi-image fluorescence microscopy for detection. Also, microfluidic based techniques for CD4 counting are developed that use optical and electrical detection techniques[2, 5, 18].

Microfabrication and microfluidic technologies have been used for a diverse set of applications in biomedical field[19-24]. In this paper, we utilize microfabrication to demonstrate a microfluidic device that uses a small-volume blood sample (1 μL) and that captures CD4 cells for counting in 3 minutes on-chip incorporating a porous filter into a microfluidic chip in order to separate and count $CD4^+$ T lymphocytes from whole blood. We present experimental results with whole blood from healthy individuals and HIV-infected subjects. We compare the results to those that are obtained by flow cytometry. This indicates the potential of such a technology for point-of-care and developing world testing combined with the necessary product development steps.

Experimental Section

The device schematic is shown in Figure 1. A mixture of fluorophore-conjugated anti-CD4 (3 μL), anti-CD3 antibodies (3 μL), whole blood (1 μL) and 1X PBS (100 μL) is initially introduced at the inlet of a microfluidic channel on the disposable device. This mixture was observed to stain the cells satisfactorily in 8-30 minutes outside the chip[4] when incubated. The herringbone structures were fabricated in the channel to speed up the mixing (<1min). This mixture enters the device through the inlet and mixes with the antibodies in the microfluidic channel by diffusion, augmented by the effect of the ridge structures depicted in Figure 1a. Channel length, flow rate and frequency of ridge structures are designed such that antibodies and whole blood mix for efficient and rapid cell staining, which occurs in approximately 30 seconds. Another 30 seconds of PBS was flowed to remove the fluorescent background due to free antibodies, increasing the contrast and quality of the collected image.

Device Design and Fabrication

Device design is presented in Figures 1a-b. Based on a simple mathematical modeling, we calculated that the baseline microfluidic circuit dimension should include a channel length larger than 5 cm, and fabricated devices with channel lengths from 5 cm to 60.5 cm to provide sufficient residence time for the cells in the device at various flow rates[23, 25]. The microfluidic channels were 500 μm wide, 200 μm high and 60.5 cm long. They were operated at flow rates up to 13.2 ml/hour. Herringbone structures 25 μm wide and 20 μm deep were placed at the channel bottom surface at a repetition frequency of 50 μm throughout the fluidic channel to facilitate mixing.

Devices were fabricated using standard micromachining techniques as shown in Figure 1c. A thin film of SU-8 photoresist was deposited onto a silicon wafer and microfluidic channels were defined by photolithography. A polydimethylsiloxane (PDMS) layer was poured on a wafer, cured at 65ºC and then bonded to another PDMS layer with the porous filter membrane placed between the two PDMS layers at the end of the microfluidic channels. Sealing between the filter membrane and the PDMS layers was achieved by the bonding process and strengthened by an hour annealing at 100 ºC. The microfluidic channels lead the labeled whole blood to a cell capture area with a polycarbonate membrane filter floor where 3 μm diameter pores (Whatman, BD Biosciences, San Jose, CA) separate and retain white blood cells while passing through red blood cells. Waste passing through the porous filter is coupled to another fluidic channel defined on the bottom PDMS layer, which leads it to an outlet from the microfluidic channel system. Waste can be collected in a reservoir for analysis of the types of filtered cells.

Device Modeling

To design devices such that antibodies and whole blood mix efficiently and rapidly in less than a minute on chip, we modeled microfluidic mixing mathematically. Microfluidic devices operate at low Reynolds numbers given by $R_e = ud/\kappa$, where 'u' is the average flow speed, 'd' is the cross-sectional dimension and 'κ' is the kinematic viscosity of the fluid. At low Reynolds numbers, mixing in channels between flows is diffusive. This diffusive mixing is slow compared to the convection of flow along the microfluidic channels. The relative rate of convective transport to diffusive transport in a channel is given by Peclet number, $P = ud/D$, where 'D' is the molecular diffusivity[23, 25]. The time required, 't', for diffusive mixing to take place in such a channel is $t = d^2/2D$. The required channel length can be estimated by multiplying this time with the average velocity of the flow, 'u'. This length can be tens of meters, which is large for a microscale device. Channel length can be reduced by introducing transverse flow components, using herringbone

structures[23, 25]. The shape width, height and periodicity of the ridges determine the mixing and can be modeled by analytical and finite element models[25].

The relative cell count estimation accuracy increases with the number of cells within the field of view. However, the probability that cell images overlap increases with cell density. Cell images that overlap cannot be classified using simple pattern recognition methods. We developed an approximate model to calculate cell overlap probability to help select the optimal size of the cell separation area. Assuming that A_{cell} is the area of a single cell and $A_{membrane}$ is the membrane area where cells are captured and imaged. Let $N_o = A_{membrane} / A_{cell}$ be the ratio of cell area to filter area. If there are N cells in an image, then the fraction of cells that do *not* overlap is $F(N) = e^{-4(N/No)}$ for $N<<No$ [26]. The number of non-overlapping cells is given by $N_{non\text{-}overlapping} = Ne^{-4(N/No)}$. To obtain acceptable performance, we developed image processing methods to separate partially overlapping cell images. These methods can handle images, where even 30% of the cells overlap. Assuming that HIV-infected individuals have between 0 and 1,000 $CD4^+$ T-lymphocytes per microliter of whole blood, and using 9 μm as a mean cell diameter for $CD4^+$ T-lymphocytes, then according to our model, 1μL of blood captured in an 800 μm×800 μm cell capture area will allow for an acceptable cell overlap of about 10% at maximum cell density of 1000 CD4 cells. This is below 30% overlap allowance limit of the image recognition software. Plotting the above equations results in figure 1d, where the non-overlapping cell percentage is plotted as a function of number of CD4 cells randomly placed on the filter area for three filter membrane sizes of 500 μm×500 μm, 800 μm×800 μm, and 1000 μm×1000 μm. For the 800 μm×800 μm filter size, the non-overlapping cell percentage is 90% for 1000 cells on the membrane. Thus, we selected this filter size for the design of the cell separation and imaging area in a device that utilizes 1 μL of whole blood.

Filter Characterization with beads and whole blood

We characterized devices first by passing beads of various size (1, 2.1, 3.1, 5, 10 μm diameter, Duke Scientific, Palo Alto, CA) through the 3 μm pore membrane in the cell separation chamber, calculating the ratio of the number of beads that passed through the filter to the total number of beads introduced. Experiments were performed at three flow rates of 50, 100 and 150 μL/min in order to characterize the influence of flow rate on bead capture efficiency.

We repeated the device characterization experiments using whole blood, since lymphocytes are viscoelastic and vary in their geometries[27]. We compared cell counts before and after 1 μL of whole blood flowed through the device at three flow rates (50, 100 and 150 μL/min). To assess cell capture efficiency, flow cytometry and Coulter counter (Beckman Coulter, Fullerton, CA) studies were performed on whole blood before and after passing through the device. The concentration of red blood cells was also recorded. For these and subsequent experiments, CD4 cell counts obtained from the device were compared to standard four-color flow cytometry (Becton Dickinson FACSCalibur, NJ). Experiments were repeated with multiple devices in order to characterize device-to-device variation.

Whole Blood Staining in Microfluidic Channels

Cells were stained with AlexaFluor 647 anti-CD3 and AlexaFluor 488 anti-CD4 antibodies (Invitrogen-Molecular Probes, Eugene, Oregon). Devices were designed to reduce the cell staining time below a minute. For subsequent experiments, fluorescent cell labeling occurred within the microfluidic channels by using fast mixing provided by the microfabricated herringbone structures. For these experiments, we initially collected 1μL of whole blood, 3μL of each antibody and 100 μL of phosphate buffered saline (1x PBS) in an eppendorf tube. The mixture was checked under a florescent microscope to see if any cell staining took place during this process in order to verify that the herringbone structures were necessary for rapid cell staining. We immediately pulled this

mixture to a 1 ml syringe and started to flow the mixture to the single inlet system as shown in figure 1a. Then, the whole blood and antibodies mixture was pushed through the microfluidic channels, where the antibody and the whole blood mix for the staining process. The stained cells were driven through the microfluidic channels into the cell separation area using PBS delivered by a syringe pump at flow rates of 50-150 µL/min. Cell labeling required ~ 30 sec at 150 µL/min. Afterwards, the channels and cells were washed for another 30 seconds with PBS, which cleared the free fluorescent antibodies from the filter surface and decreased the fluorescent background. Fluorescent images of the retained lymphocytes were collected and transferred to custom cell counting image recognition software. CD4 count results were obtained within ~3 minutes.

Imager Design

After the cell separation step, cells retained in the device were imaged directly. A compound fluorescence microscope (Nikon Eclipse TE2000, Nikon, Japan) with a 10X objective lens (Nikon, Japan) was used for imaging. The imaging area on the chip fit a single image of the imaging system. The filters and light sources were set for fluorescence imaging at the two wavelengths emitted by the fluorophores used to label cells, AlexaFluor 488 and AlexaFluor 647. A fluorescent microscope and a commercial charge-coupled device imager (CCD, Rtke 229317, Diagnostic Instruments) were used for image capture in 'tif' format.

Image Processing and $CD4^+$ Cell Counting Algorithm

For each experiment, we obtained two images of the cell separation area on chip at the two emission wavelengths. After images were collected, custom image recognition algorithms based on matched filtering, binary image processing, moment calculations and pattern classification were used to identify each object based on object parameters such as area, perimeter, inertia, brightness, and eccentricity. The software checked the Euler number of the images to determine whether the fluorescent cell images had dark spots that would disqualify the fluorescent bright spot as a cell image. Perimeter and area of objects defined as bright spots were calculated in order to determine if the object agreed with the expected cell diameter range of the T lymphocytes (8-10 µm). Finally, shape factors, including eccentricity and inertia, were calculated in order to determine whether a suitably bright "image blob" presented the shape expected of fluorescent cell images. Adaptive techniques were used to account for variations in background and cell image brightness variations across the field of view. In establishing the local background, image processing techniques were used to suppress contributions from nearby, touching, or overlapping cells.

CD4 Counts with Whole Blood

Initially, to optimize the device, unprocessed whole blood was obtained from healthy volunteers, flowed through the device and cell counts were determined in at least 3 devices and compared to flow cytometry results obtained by using the same whole blood sample. In order to verify that the device behaves similarly with clinical specimens, we obtained whole blood samples from five HIV-infected subjects. For each subject, accuracy and variability were assessed by experiments in three to ten separate devices. The Bland-Altman method was employed to compare the flow cytometry results with the microfluidic system results[28]. All subjects were recruited from the Massachusetts General Hospital and provided informed consent. Flow cytometry for HIV-1 infected subjects was performed at the Massachusetts General Hospital clinical laboratories, and for healthy volunteers at the research laboratory, using standard four-color protocols on a BD FACSCalibur.

Results

Device Design

We established three design specifications essential for point-of-care measurement of CD4+ T lymphocytes under fluorescence imaging. First, robust and rapid cell staining with two fluorescent anti-CD4 and anti-CD3 antibodies is achieved. The use of both labels allows differentiating CD4+ T lymphocytes (CD4+/CD3+) from monocytes (CD4+/CD3-). Second, all white blood cells must be captured on the filter. Third, optimal device operation would rely on a minimum number of moving parts. Hence, an image captured at a single location by a CCD or CMOS imager sufficient to make accurate counts of CD4+ T lymphocytes per unit volume would be preferable.

Our device design comprises three elements combined on a single chip: (i) passive microfluidic channels, where two antibody reagents mix with whole blood by diffusion-facilitated mechanical stirring in order to rapidly stain cells; (ii) a passive mechanical filter that captures all white blood cells and allows most of the red blood cells to pass through. Filter also serves as a flat plane for washing off excess antibodies and for fluorescence imaging; and (iii) an imaging chamber, in which the mechanical filter membrane resides, sized appropriately to allow capture of CD4+ T cells for statistically valid counting in a single imaging field. For optimal performance, the device would be used in conjunction with a low-cost fluorescence imaging system and an embedded image recognition algorithm to count $CD4^+$ and $CD3^+$ cells from a single acquired image.

To calculate the surface area and volume of cell capture and imaging chamber in which the mechanical membrane filter sits, we first established that the imaging area should be small enough to allow a single image to be taken and be used to determine the number of $CD4^+$ T-lymphocytes (i.e., $CD4^+$ and $CD3^+$ leukocytes) per unit volume of blood. For large filters, post structures would be necessary to keep the filter plane (i.e., the imaging plane) flat to achieve good focusing. Thus, the size of the filter should be such that it is easily fabricated, small enough not to require stabilizing posts, yet large enough to accommodate enough cells for a statistically valid cell count, and at a reasonable cell density. The cell packing should avoid excessive overlap. Otherwise, it be difficult to classify by the image recognition algorithm. For calculations, we assumed that lymphocytes are on average 9 μm in diameter, and a dynamic range of 0-1,000 cells/μL of whole blood. We were less concerned with error at the high end of the range, since clinically relevant CD4 counts are at the lower end of the range. Thus, we allowed for up to about 30% overlap of cells in the worst-case scenario. Our analytic model (see the Methods section) established 800 μm x 800 μm dimensions as an appropriate imaging chamber/membrane filter size for 1 μm of whole blood (Figure 1b).

Experimental characterization of devices

Figure 2 illustrates experimental results with our microfluidic device. Behavior of beads of various sizes using a mechanical filter with a 3μm diameter pore size is presented in Figure 2a. Beads of 1μm and 2.1μm diameter passed through the filter, and we observed no beads on the filter surface. The efficiency of mechanical filtration was sensitive to bead size, but independent of flow rates. By contrast, 5μm and 10μm diameter beads did not pass through the 3μm diameter pore size membrane, and accumulated on the membrane surface. The calculations involving the division of 800μmx800μm area by the 5 μm diameter bead cross-sectional area indicate that approximately 25,600 beads would cover the whole imaging area with a single monolayer. The imaging area was observed to be completely filled with fluorescent beads in several layers, when more than $1x10^6$ beads of 5 μm diameter were placed on the membrane surface. Although the membrane imaging area was observed to be filled with beads and the microfluidic channel resistance increased, fluid flow was continuous, indicating that fluid flowed through the gaps between beads. Fluid that passed through the filter was collected on the other end, which did not contain 5μm or 10μm beads

when fluorescent imaging was performed on the waste fluid. 10%, 12%, 15% of 3.1 μm diameter beads, a diameter comparable to the 3μm diameter pore size, passed through the device at flow rates of 50 μL/min, 100 μL/min, and 150 μL/min, respectively (figure 2). The flow rate had a small impact on the percentage of beads that pass through the filter, as higher flow rates caused a slight increase in the fraction of beads that pass through the filter.

We repeated these characterization experiments with whole blood, comparing cell count results before and after 1 μL of whole blood passed through the device, as demonstrated in Figure 2b. The majority of red blood cells, smaller and more deformable than white blood cells, were observed to pass through the filter. White blood cells accumulated on the membrane surface. Moreover, increased flow rates increased the percentage of red blood cells that passed through the filter, likely due to increased shear and pressure in the microfluidic channel and across the filter. Flow cytometry was performed on the filter flow-through to verify white blood cell capture. The results indicated that none of the white blood cells passed through the polycarbonate filter and that most of the red blood cells passed through the filter. Although a high percentage of red blood cells (up to 80%, figure 2b) passed through the filter, the remaining number of red blood cells on the filter corresponded to less than one million red blood cells and multiple erythrocyte layers (~50) on the filter area. This is expected to cause light scattering, but the presence of residual red blood cells on the filter did not interfere with fluorescent imaging (Figure 3). This was also earlier reported by Rodriguez *et al.*[4].

Rapid cell staining is essential to high throughput device operation. Staining of cells in our device by herringbone structure augmented diffusion, using 3 μL of each antibody and 1 μL of whole blood, was achieved in 30 seconds, at a flow rate of 50-150 μL/min through the 60.5 cm long 200 μm high and 500 μm wide channel. The quality of the fluorescent staining could be easily evaluateds by determining the fluorescent intensity and shape of the cells under the fluorescent microscope.

CD4 counts from whole blood samples

Figure 3 demonstrates typical results obtained by fluorescence imaging and cell counting. The first two subpanel images of figure 3a are raw images taken such that cells that only stain with Alexa-647 anti-CD3 antibody correspond to $CD3^+$ T-cells and appear red. Cells that only stain with the Alexa-488 CD4 antibody correspond to monocytes and appear green. Cells that stain with *both* antibodies correspond to $CD4^+$ T cells of interest, and appear yellow. Later, the two raw images were merged and processed using image recognition techniques and total number of CD4 T cells was identified automatically. The $CD4^+$ $CD3^-$cells are circled in green, the $CD4^-$ $CD3^+$ are circled in red, where the $CD4^+$ $CD3^+$ cells are circled in yellow and are counted as shown in Figure 3b. The image recognition algorithm was observed to differentiate cells that overlap by as much as 30% of their area by (i) recognizing that cells overlap, and (ii) splitting the partial images of the overlapping cells and (iii) estimating properties of the obscured part of each of the two cell image. The limit of this approach was reached when the cell density became so high that clusters of more than two cells abound. The number of such clusters grows quadratically with cell density.

We next compared CD4 counts obtained by our device with counts obtained by flow cytometry for HIV-infected subjects (Figure 3c). In Figure 3c, Bland-Altman method comparison analysis is employed, which indicates acceptable 95% limits of agreement. First, we worked with 10 healthy samples and each blood sample was run on at least 3 separate devices and the results placed on the figure as circular dots. The data for one such typical sample from a healthy subject is presented in figure 3c at 900 cells/μL count level. This established the fact that the device could handle whole blood and device variability did not appear to affect the count results, indicating that we can

fabricate devices repeatably. This finding was confirmed by running a single healthy blood sample up to 10 separate devices and obtaining similar CD4 counts at the high end cell count range, where factors such as cell overlap errors are expected to be maximal. These results also indicated that whole blood mixed with antibodies could be directly applied to the device without any other prior processing. Second, to verify that the device could handle HIV infected blood and produce similar results to the healthy samples, we compared microchip results to those from flow cytometry for 4 HIV infected patients with CD4 counts <600 cells/μL (Figure 3c). The dotted gray lines indicate the 95% confidence limits. Each sample was run on at least 3 separate devices. This lead to the fit "y=0.96x+13.95". Most of the count results are within the 95% confidence interval indicating the accuracy of the device, which is beyond the 80% accuracy limit that would be satisfactory for initial useful employment of such a device in resource limited settings. To summarize the results, a total of 15 samples (including the healthy individuals) were run at least on 3 separate devices and as many as 10 devices per sample. The CD4 count data was collected from each device and compared to the flow cytometry data, which is the gold standard. Although the microchip devices were observed to perform similarly with patient blood and with healthy donor samples, it is necessary to increase the sample set especially for HIV patient samples.

Discussion

The results indicate that a microfluidic device combined with fluorescence imaging and digital image analysis can be successfully utilized for obtaining CD4 cell counts in whole blood in less than 3 minutes, and with minimal sample preparation.

The mathematical model developed to determine the optimal size of the cell separation area and sample volume could be improved by adding the influence of the pore location on the membrane, which affects the cell distribution on the membrane. In our device, we utilized a commercially available filter for convenience. In a mature device, pores could be micromachined[29] in batch format with pore size and periodicity controlled by standard lithographical methods[30, 31]. The membrane could be fabricated out of materials such as silicon, silicon nitride, or silicon oxide[32].

We compared the accuracy of our device to standard flow cytometry in a population of adults. CD4 counts from 0 to 1,000 cells/μL represent the clinically relevant CD4 range, with the critical clinical threshold at 200 cells/ μL. First, our experimental results with whole blood from healthy individuals suggest that microfluidic devices used for cellular analysis can be accurate within a ±10% error margin compared to clinical flow cytometry[11, 33]. For high CD4 counts, the CD4 cells are more likely to overlap, which may introduce additional error and limit the applicability of this method to higher ranges of cell counts above 1000 cells/μL. This limitation could be overcome by increasing the filter area during microfabrication, since the sample distribution on the filter is controllable and accurate volumetric control is possible by microfluidic techniques. Second, we used the device with HIV infected patient samples using directly unprocessed whole blood and showed that the device worked with those samples as well. However, further experiments in a larger, more diverse group should be performed in order to reaffirm the accuracy of the method, including an assessment of assay bias and reproducibility. Trials in resource-limited settings with an automated prototype would also be necessary. Moreover, we did not follow overall intensity measurements, since it may not be reliable and repeatable to quantify the number of cells due to possible degrading of fluorescence. The process needs both CD3 and CD4 fluorescence. The imaging and quantification approach that we used is more reliable in terms of identifying labeled cells independent of their fluorescent intensity as long as they are visible by the system. We used two images taken at the filter area of the device and utilized the image recognition software to attempt to identify overlapping cells. The theory and overlap efficiency limits are discussed earlier.

The image quality, count variation and error range were similar in results obtained for HIV-infected patient samples or for healthy samples. However, further patient blood experiments would be necessary in order to confirm this observation. For studies of whole blood obtained from human subjects, a fluorescence imaging system optimized for low power consumption and low cost can be manufactured[34-36]. Key engineering trade-offs in the design should be considered. First, a low-cost CMOS imager could be utilized. Second, low cost and long-life light emitting diodes (LED's) and laser diodes could be used for illumination. Third, a single multi-layer dielectric filter that passes 519 nm and 668 nm wavelength light could be used in front of the imager, allowing relatively inexpensive optical components (mirrors, lenses, filters) to be used in the rest of the optical design. These components are available and a prototype imager can be designed for fluorescence imaging at the two wavelengths emitted by the fluorophores used to label cells, AlexaFluor 488 and AlexaFluor 647. Given the low illumination and CMOS imager, the prototype imager would use 30 seconds exposure time for image capture, which would not significantly increase assay time. Although UV (365 nm) LEDs may still cost around US$100, high intensity LEDs emitting at wavelengths between 400 and 650 nm are available in single quantities for less than US$5. The plastic optics used for illumination and light collection in LED-illuminated image cytometers are inexpensive. Interference filters are likely to be the most costly components of the optical system, and these should cost less than $50.

Additional engineering work on optics by using LEDs and increasing robustness of the device optics, optimization of simple electronics for battery-powered operation, design of mechanical components for easy operation, optimization of the microfluidic system would make a point of care instrument for field testing. The current devices were fabricated using PDMS technology for quick prototyping and analyzing the device performance and capabilities at an initial level. The repeatability and mass production of the device would be enabled by building the device using injection molded plastic or alike polymers. Furthermore, the device also has the potential to give CD4 percentages of T lymphocytes (CD4:CD8 ratios) for pediatric monitoring.

Although most lab-on-a-chip devices are focused on applications in developed countries, this device demonstrates that application of microfluidic techniques could offer several advantages in order to bring solutions to limitations of performing diagnostic assays in resource-limited settings of the developing world. For instance, capability to work with small samples enables working with fingerstick samples of blood, which diminishes the need for venipuncture, minimizes medical waste, and exposure to biohazardous material. Also, the amount of reagents used and the cost associated with these is minimized. Moreover, labor- and equipment-intensive sample preparation steps and costs associated with those steps are eliminated. Elimination these steps increases the throughput. This system has the potential to increase throughput significantly to as fast as 60 seconds per patient, which could enable real time clinical decisions at the point of care.

Acknowledgements

We would like to thank Dr. Bart Kane and Prof. Edward Hæggstrom for invaluable discussions. We would like to thank Mr. Octavio Hurtado for his generous support. This work was performed at Charlestown-MGH, Harvard Medical School. It was partially supported by the National Institute of Biomedical Imaging and Bioengineering under Grant No. P41 EB002503 (BioMEMS Resource Center). Dr. William Rodriguez was supported by grants from the National Institutes of Health, the Bill and Melinda Gates Foundation, and the Doris Duke Charitable Foundation.

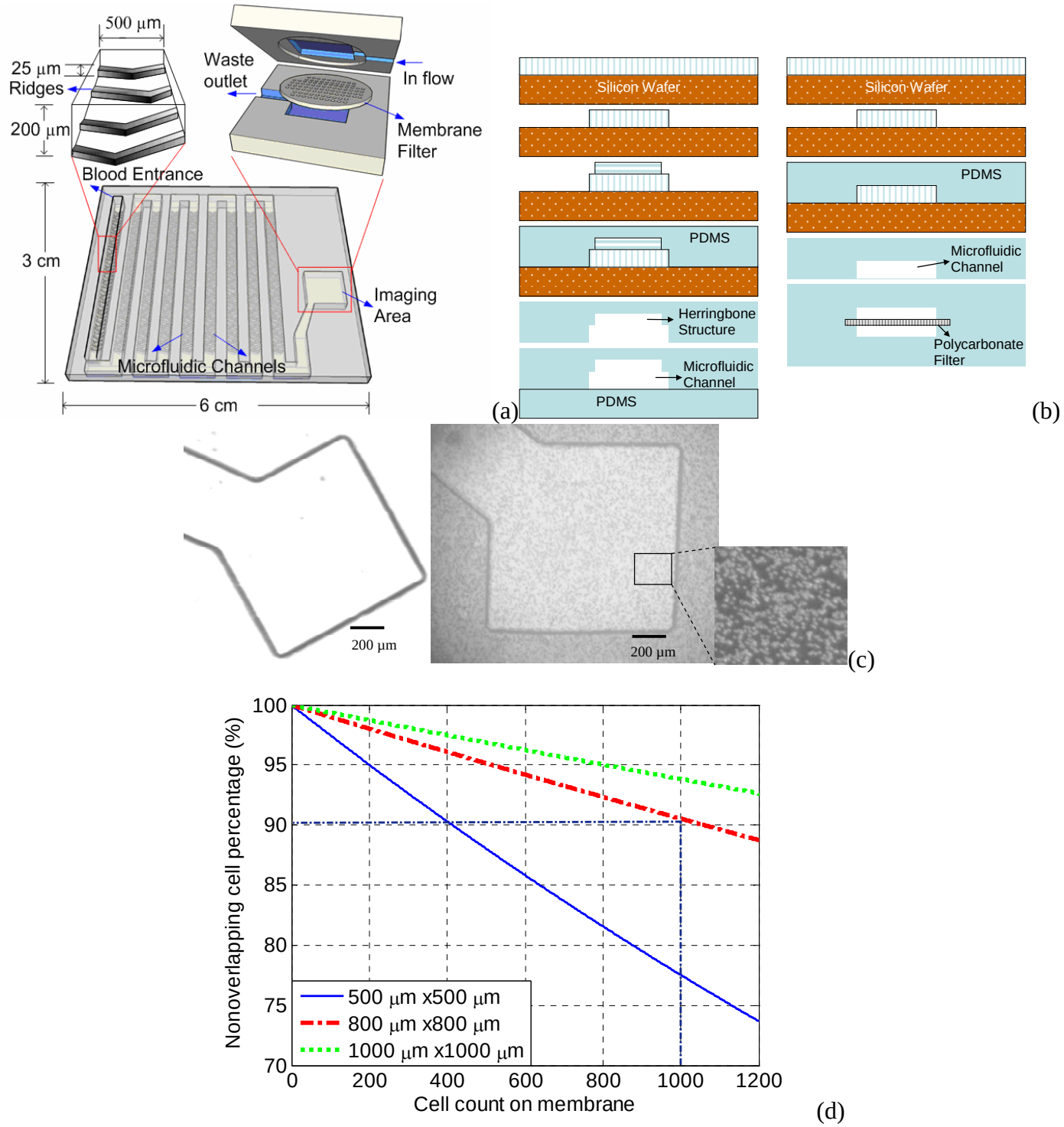

Figure 1. (a) The microfluidic channel design ending at the filter. The antibodies and whole blood are mixed by ridge structures located at the bottom of the channel. A magnified schematic of the filtering and imaging area of the device with the waste disposal channels is shown. (b) The schematic of the fabrication steps for the microfluidic channel fabrication with herringbone structures and the on-chip filtering area with a polycarbonate filter. (c) The disposable microfluidic device, 800 µm x 800 µm area on membrane where the cells accumulate or pass through the filter as observed from the top by a CCD camera with and without filter membrane. (d) Mathematical modeling for analysis of overlap of cells for 800 µm x 800 µm area predicts approximately 10% overlap at the worst case scenario. 1µL of blood gives counts between 0-1000 cells. This is an acceptable volume of blood for the designed filter area size.

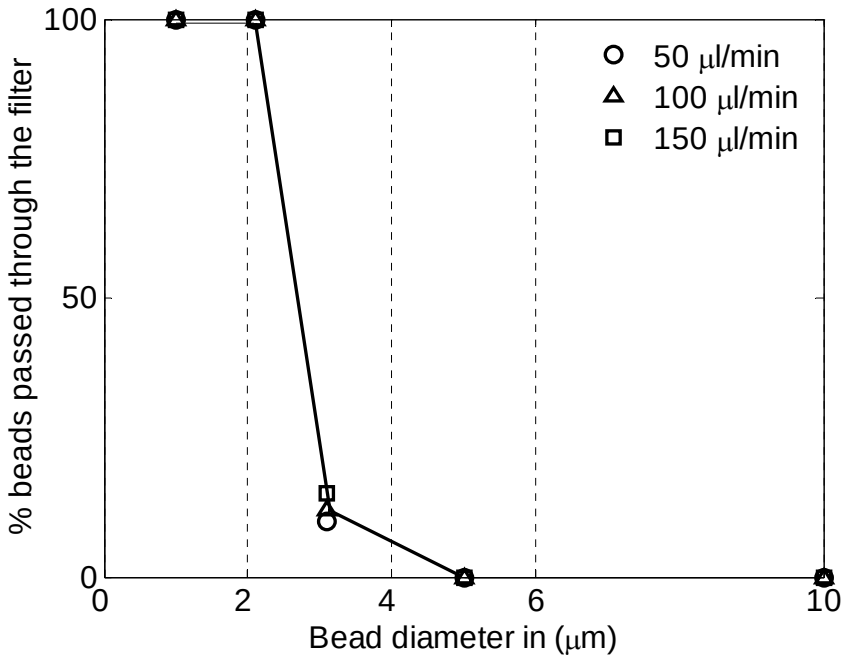

(a)

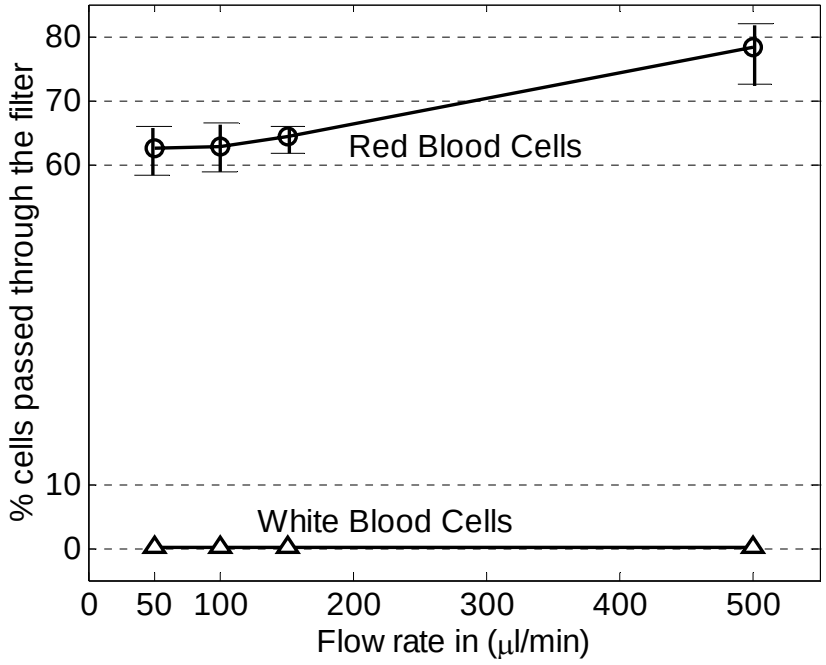

(b)

Figure 2. (a) Flow rate vs. percentage of beads of various sizes (1, 2.1, 3.1, 5, 10 μm diameter) that pass through a 3 μm diameter pore size membrane, (b) Experimental results that characterize the percentage of red blood cells and white blood cells that pass through the filter at three flow rates.

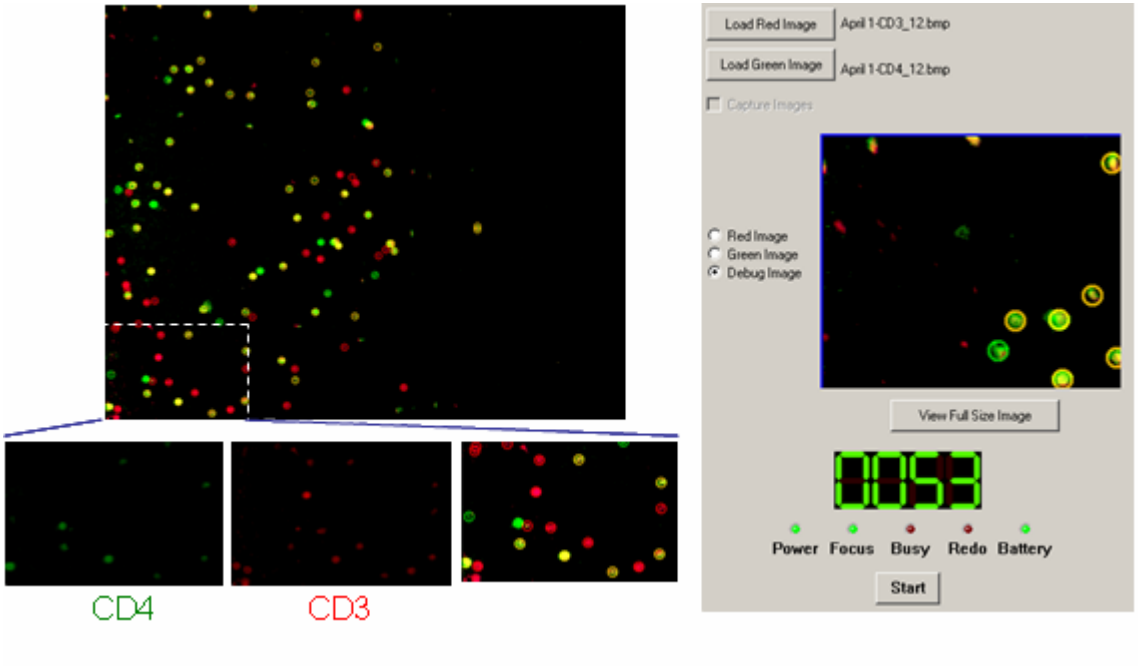

(a) (b)

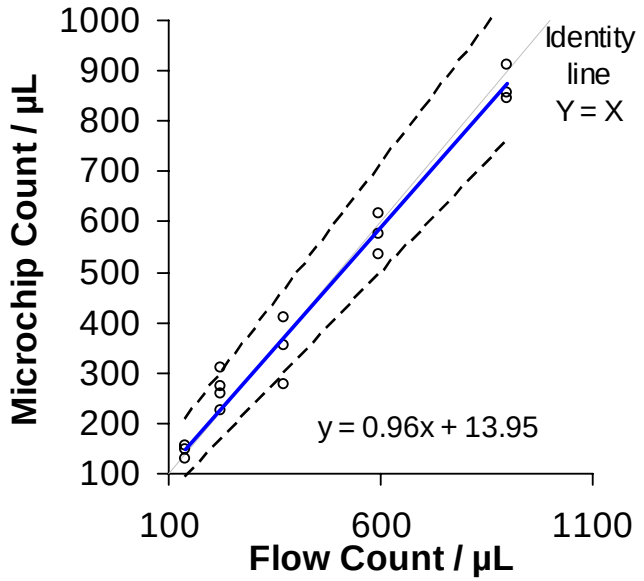

(c)

Figure 3. These figures are obtained by using unprocessed whole blood. (a) Each location on the image is identified, where red marked cells correspond to $CD3^+$ cells, green marked cells correspond to $CD4^+$ cells and the yellow marked locations on the image correspond to $CD3^+$ and $CD4^+$ T-lymphocytes. (b) The software output is shown, the yellow circles are automatically drawn by the image recognition software and the $CD4^+$ T-cell count is displayed as '53'. (c) The horizontal axis corresponds to the measurements by the flow cytometers, which is the gold standard. The vertical axis corresponds to the CD4 counts for the same blood sample obtained by the microchip. Each circular point is a separate microchip device result obtained for a blood sample. Multiple circular points for the same flow cytometry count indicates that the same blood sample was run over multiple microchips in order to obtain statistical information. Grey line indicates zero bias and dotted lines indicate 95% limits of agreement. CD4 cell count comparison of results of analysis of blood samples from one healthy and 4 HIV infected donors, plotted as "Flow Count" vs. "Microchip Count.

References

(1) Cohen, J. *Science* **2004**, *304*, 504-509.
(2) Cheng, X.; Irimia, D.; Dixon, M.; Ziperstein, J. C.; Demirci, U.; Zamir, L.; Tompkins, R. G.; Toner, M.; Rodriguez, W. R. *J Acquir Immune Defic Syndr* **2007**.
(3) Butte, M. J.; Wong, A. P.; Sharpe, A. H.; Whitesides, G. M. *Clinical Immunology* **2005**, *116*, 282.
(4) Rodriguez, W. R.; Christodoulides, N.; Floriano, P. N.; Graham, S.; Mohanty, S.; Dixon, M.; Hsiang, M.; Peter, T.; Zavahir, S.; Thior, I.; Romanovicz, D.; Bernard, B.; Goodey, A. P.; Walker, B. D.; McDevitt, J. T. *PLoS Medicine* **2005**, *2*, e182.
(5) Cheng, X.; Irimia, D.; Dixon, M.; Sekine, K.; Demirci, U.; Zamir, L.; Tompkins, R. G.; Rodriguez, W.; Toner, M. *Lab Chip* **2007**, *7*, 170-178.
(6) Cheng X, L. Y., Irimia D, Demirci U, Yang L, Zamir L, Rodriguez WR, Toner M, Bashir R. *Lab Chip* **2007**, *7*, 746-755.
(7) Balakrishnan P, D. M., Kumarasamy N, Crowe S, Subbulakshmi G, Ganesh AK, Cecelia AJ, Roth P, Mayer KH, Thyagarajan SP, Solomon S **2004**, *36*, 1006-1010.
(8) Cohen, J. *Science* **2004**, *304*, 1936.
(9) Linder, V.; Sia, S. K.; Whitesides, G. M. *Analytical Chemistry* **2005**, *77*, 64-71.
(10) Patient Monitoring Guidelines for HIV Care and ART, W.; Health Organization, N., 2005, available at http://; www.who.int/hiv/pub/guidelines/patientmonitoring.pdf, a.; 2006., t. M.
(11) Dieye, T. N., C. Vereecken, A. A. Diallo, P. Ondoa, P. A. Diaw,; M. Camara, F. K., S. Mboup and L. Kestens *Journal of Acquired Immune Deficiency Syndromes* **2005**, *39*, 32-37.
(12) Josefowicz, S. Z.; Buchner, L.; Epling, C. L.; Sinclair, E.; Bredt, B. M. *Cytometry* **2004**, *59A*, 124.
(13) Kannangai, R.; Prakash, K. J.; Ramalingam, S.; Abraham, O. C.; Mathews, K. P.; Jesudason, M. V.; Sridharan, G. *J Clin Virol* **2000**, *17*, 101-108.
(14) Landay, A.; Ho, J. L.; Hom, D.; Russell, T.; Zwerner, R.; Minuty, J. G.; Kataaha, P.; Mmiro, F.; Jackson, B. *AIDS* **1993**, *7*, 1565-1568.
(15) Didier, J. M.; Kazatchkine, M. D.; Demouchy, C.; Moat, C.; Diagbouga, S.; Sepulveda, C.; Di Lonardo, A. M.; Weiss, L. *J Acquir Immune Defic Syndr* **2001**, *26*, 193-195.
(16) Lyamuya, E. F.; Kagoma, C.; Mbena, E. C.; Urassa, W. K.; Pallangyo, K.; Mhalu, F. S.; Biberfeld, G. *J Immunol Methods* **1996**, *195*, 103-112.
(17) S. Crowe, S. T., R. Oelrichs and A. Dunne *Clin. Infect. Dis.* **2003**, *37*, S25-S35.
(18) Cheng, X.; Liu YS, I. D., Demirci U, Yang L, Zamir L, Rodriguez WR, Toner M, Bashir R. *Lab Chip* **2007**, *7*, 746-755.
(19) Demirci, U. *Journal of Microelectromechanical Systems* **2006**, *15*, 957- 966.
(20) Whitesides, G. M.; Ostuni, E.; Takayama, S.; Jiang, X.; Ingber, D. E. *Annu Rev Biomed Eng* **2001**, *3*, 335-373.
(21) Voldman, J.; Gray, M. L.; Schmidt, M. A. *Annu Rev Biomed Eng* **1999**, *1*, 401-425.
(22) Demirci, U.; Ergun, A. S.; Oralkan, O.; Karaman, M.; Khuri-Yakub, B. T. *IEEE Transactions on UFFC* **2004**, *51*, 887-895.
(23) Stroock, A. D.; Dertinger, S. K.; Ajdari, A.; Mezic, I.; Stone, H. A.; Whitesides, G. M. *Science* **2002**, *295*, 647-651.
(24) Demirci, U. *Lab Chip* **2007**, *DOI:10.1039/B704965J*.
(25) Sethu, P.; Anahtar, M.; Moldawer, L. L.; Tompkins, R. G.; Toner, M. *Analytical Chemistry* **2004**, *76*, 6247-6253.
(26) Leon-Garcia, A. *Probability and Random Processes for Electrical Engineering*, 2nd ed.; Addison-Wesley, 1994.

(27) Panaro, N. J.; Lou, X. J.; Fortina, P. *PCR Biomolecular Engineering* **2005**, *21*, 157-162.
(28) Bland, J. M.; Altman, D. G. *Stat Methods Med Res* **1999**, *8*, 135-160.
(29) Demirci, U.; Toner, M. *Applied Physics Letters* **2006**, *88*.
(30) Demirci, U.; Yaralioglu, G. G.; Haeggstrom, E.; Khuri-Yakub, B. T. *IEEE Transactions On Semiconductor Manufacturing* **2005**, *18*, 709-715.
(31) Demirci, U.; Yaralioglu, G. G.; Haeggstrom, E.; Percin, G.; Ergun, S.; Khuri-Yakub, B. T. *IEEE Transactions On Semiconductor Manufacturing* **2004**, *17*, 517-524.
(32) Demirci, U.; Ozcan, A. *Electronics Letters* **2005**, *41*, 1219-1220.
(33) Lopez, A.; Caragol, I.; Candeis, J.; Villamor, N.; Echaniz, P.; Ortuno, F.; Sempere, A.; Strauss, K.; Orfao, A. *Cytometry* **1999**, *38*, 231-237.
(34) Li, X. T., A. G. J.; Droog, E.; Terstappen, L. W. M. M.;Greve *J. Clin Vaccine Immunol* **2007**, 412-419.
(35) Li, X. e. a. *Cytometry* **2007**, in press (doi://10.1022/cyto.b.20165).
(36) Ymeti, A. L., X., Lunter, B., Breukers, C., Tibbe, A.G.J.,Terstappen, L.W.M.M., & Greve, J. *Cytometry* **2007**, *3*, 132-142.